Volume 22
Number 22
21 November 2020
Pages 7569-8048

Green Chemistry

Cutting-edge research for a greener sustainable future

rsc.li/greenchem

ISSN 1463-9262

ROYAL SOCIETY OF CHEMISTRY

PAPER

Youngho Eom, Sung Yeon Hwang, Jun Mo Koo *et al.*
Remarkable elasticity and enzymatic degradation of bio-based poly(butylene adipate-*co*-furanoate): replacing terephthalate

Green Chemistry

PAPER

View Article Online
View Journal | View Issue

Cite this: *Green Chem.*, 2020, **22**, 7778

Remarkable elasticity and enzymatic degradation of bio-based poly(butylene adipate-*co*-furanoate): replacing terephthalate†

Hyeri Kim,‡[a] Taeho Kim,‡[a] Sejin Choi,[a] Hyeonyeol Jeon,[a] Dongyeop X. Oh,[a,b] Jeyoung Park,[a,b] Youngho Eom,*[c] Sung Yeon Hwang *[a,b] and Jun Mo Koo *[a]

Biodegradable polyesters, such as poly(butylene adipate-*co*-terephthalate) (PBAT), can trigger the hydrolysis of esters in a natural environment. However, biodegradability does not guarantee its eco-friendliness due to the concerns associated with terephthalic acid. Substitution by biomass-based counterparts no longer ensures "truly" eco-friendly biodegradable polyesters. In this study, we have used poly(butylene adipate-*co*-furanoate) (PBAF), which utilizes a biomass-derived substituent, furan-2,5-dicarboxylic acid (FDCA), and have proven that this is superior from the perspective of both mechanical performance and enzymatic degradation. Compared to its terephthalate counterpart, PBAF exhibits remarkable elasticity upon stretching: when released beyond 800% extension, PBAT almost malfunctioned, whereas PBAF exhibited instant elastic recovery. This results in PBAT and PBAF having a similar tensile strength in the range of 50–70 MPa at the ring fraction of 50 to 80 mol%. During the enzymatic degradation using lipase from *Thermomyces lanuginosus*, PBAF with a ring fraction of 50 mol% solely undergoes hydrolysis due to enzyme specificity. *Ex situ* spectroscopic analysis confirms that the participation of FDCA ester groups in the early stages of degradation triggered the successive hydrolytic reaction. Thus, understanding the structural characteristics of FDCA would open new opportunities in the field of sustainable plastic industries.

Received 19th May 2020,
Accepted 14th July 2020

DOI: 10.1039/d0gc01688h

rsc.li/greenchem

Introduction

Plastic, a petroleum product, was once regarded as an essential commodity, primarily because of its widespread applications and its convenience of use. In fact, the damage caused by petroleum products and their wastes was easily overlooked. Currently, however, the effects of cumulative plastic pollution on soil, atmosphere, and marine ecosystems have become extremely severe, affecting everyday lives, and are a legitimate threat to future generations.[1–5] Consequently, efforts are being made globally to ban plastic disposal into the sea/landfills and restrict its incineration, while exploring an alternative that has the advantages of plastic. Understanding the importance of developing biodegradable and sustainable plastics has never been higher.[6–13]

Commercially available biodegradable plastics, such as poly(lactic acid), have already made an impact on the plastic industries that changed the course of polymer developments. Such success has encouraged the world to explore new biomass based materials that can improve existing polymers. One of the representative examples of a biodegradable polymer that can have high potential for substituents is poly(butylene adipate-*co*-terephthalate) (PBAT), which is commercially known as Ecoflex®, Wango, and Eastar Bio.[14] It is an aliphatic–aromatic copolyester whose crystallinity, mechanical properties, and biodegradability can be changed by controlling the composition ratio of its aliphatic and aromatic contents.[15,16] Generally, a 50 : 50 ratio of the aromatic and aliphatic contents is maintained during the synthesis of PBAT, in order to have tear resistance, flexibility, and water resistance similar to those of low-density polyethylene.[17,18] This is to ensure that the former can be used for making various products such as food packaging materials,[19–21] mulching films,[22–24] and biomedical materials.[25–27]

However, PBAT is a petroleum-based polyester that leaves behind non-consumable and toxic monomers after degra-

[a]*Research Center for Bio-based Chemistry, Korea Research Institute of Chemical Technology (KRICT), Ulsan 44429, Republic of Korea. E-mail: crew75@krict.re.kr, jmkoo@krict.re.kr*
[b]*Advanced Materials and Chemical Engineering, University of Science and Technology (UST), Daejeon 34113, Republic of Korea*
[c]*Department of Polymer Engineering Pukyong National University, Busan, 48513, Republic of Korea. E-mail: eomyh@pknu.ac.kr*
†Electronic supplementary information (ESI) available: Experimental section and complete characterization data. See DOI: 10.1039/d0gc01688h
‡These authors contributed equally.

dation, particularly terephthalic acid (TPA). TPA is a chemically synthesized monomer that is ranked in the top 50 most abundantly produced chemicals worldwide.[28] It is one of the most commonly used monomers for producing polyesters such as poly(ethylene terephthalate) (PET) and poly(butylene terephthalate) (PBT). However, the synthesis of TPA produces byproducts that affect the environment and human health.[29–33] Hence, effective substitutes for TPA are being explored to overcome its limitations.

Amongst the possible candidates, biomass derived furan-2,5-dicarboxylic acid (FDCA) is the most potential substitute due to the similarities in its structural, chemical, and physical properties to those of TPA.[34–39] However, in contrast to the highly symmetric and planar structure of TPA, which has π–π stacking,[40] the molecular packing in FDCA is lost due to an inherent angle of 129.4° between the carboxylates. Yet, it adopts a spiral motif and a diverse nonlinear architecture within a polymer chain and acquires attractive properties.[41] To compare FDCA directly with TPA, it is important to understand the physical and chemical roles of FDCA within the polymer chain.

Numerous studies on the biodegradation behavior of FDCA-based polyesters have investigated the macroscopic transitions and function of counterparts and have discussed the consequential interpretations.[42–46] However, a comparative and fundamental understanding of the structural role of FDCA and its effect on the biodegradation mechanism is crucial to validate the expansion of its applications.

To mitigate plastic pollution and to substitute TPA-based polyesters, we conducted a comparative study to reveal the structural role and benefits of using FDCA. We proposed a FDCA-based polyester, poly(butylene adipate-*co*-furanoate) (PBAF), whose synthetic protocol would be identical to that of PBAT. PBAF was expected to exhibit competing mechanical properties and superior degradability. Thermal studies of the two polyesters revealed the effects of structure and composition on the crystallization and melting behaviors. The analysis, in turn, aided in interpreting the unique degradation behavior in chemical and enzymatic media. The sequence of degradation and the transitions during the degradation were determined through two-dimensional correlation spectroscopy (2DCOS),[47–49] in order to understand the contribution of the FDCA moiety in the enzymatic degradability of PBAF. The segmental motion of chains and kinetic parameters such as the activation energy were investigated using dynamic mechanical analysis (DMA) and the corresponding Arrhenius plot, respectively, to gain insights into the molecular affinity and thermodynamics of the polymer–enzyme system during degradation.

Results and discussion

Synthesis of poly(butylene adipate-*co*-furanoate) with remarkable mechanical elasticity

Two series of copolyesters, using petrochemical and bio-based monomers, were synthesized by a conventional two-step melt polymerization method, such that all the synthesized copolyesters had a similar molecular weight (M_n) of ±3000 g mol^{-1}. The polymerization procedure and results are shown in Fig. 1a and Table S1.† In this synthesis, the dimethyl forms of TPA (dimethyl terephthalate, DMT) and FDCA (dimethyl-2,5-furandicarboxylate, DMFD) were used, while maintaining the molar ratio of methyl carboxylate to 1,4-butanediol (BD) at 1.6. The ester-exchange reaction occurred at two temperatures, 180 and 210 °C, owing to the reactivity difference of the methyl and hydroxyl leaving groups. Initially, the reaction was conducted at 180 °C to allow the complete reaction of DMT/DMFD with BD, ensuring the expected aromatic composition ratio and preventing severe discoloration. Finally, the temperature was increased to 210 °C to allow the reaction of the remaining adipic acid (AA). Despite the separate ester-exchange stages, the transesterification mechanism ensured that the copolyester is a random copolymer. The composition ratio of each copolyester was determined from the ^{1}H NMR spectrum, in which the integrated ratio of the peaks (Fig. S1 and Table S1†) was calculated to show that the composition ratio matches with the feed ratio.

To support and establish that the sequence of copolyesters is random, sequence distribution was calculated (Table S2 and Fig. S2†). As can be seen in Table S2,† the randomness '*R*' converges to the value of 1, confirming that the distribution obeys Bernoullian statistics. If $R < 1$, = 1, = 2, and = 0, it means that the polymer is a block copolymer, random copolymer, alternating copolymer, homopolymer, respectively.[50,51] Therefore, the result confirms that synthesized copolyesters are completely random.

The poorer mechanical properties of PBAF as compared to PBAT are expected, considering that FDCA has an asymmetric, semi-rigid structure while TPA is symmetric (Fig. S3†). Although the low-strain property (*i.e.*, Young's modulus) met the aforementioned expectation, surprisingly, the high-strain property (*i.e.*, tensile strength) was comparable between the two polymers. Fig. 1b, c and S4 and Table S3† show that the tensile strengths of both the copolyesters increase with increasing aromatic content because a higher ring fraction imparts a stiffer chain structure. The tensile modulus of PBATs is almost 1.5 times greater than that of PBAFs (Fig. 1b). However, the ultimate tensile strength of PBAFs is comparable to that of PBATs and ranges from 49.2 to 74.7 MPa at a ring fraction of 50–80 mol%. This suggests that the strain-induced chain orientation and the lateral alignment compensate for the inferior chain regularity of PBAFs. Thus, the difference in the mechanical performances of the two copolyesters becomes narrow, and finally negligible, with increasing tensile strain. It is worth noting that the stiffening of the stretched PBAF chains alone cannot completely explain the high mechanical strength.

A huge difference in the elastic recovery is observed when the copolyesters are released after 800% stretching. While PBAT50 (aromatic content of 50 mol%) lost its mechanical performance due to an irreversible deformation, PBAF50 exhibited instant elastic recovery (Fig. 1d and Movie S1†). It is obvious that this remarkable elasticity amplifies the resistance

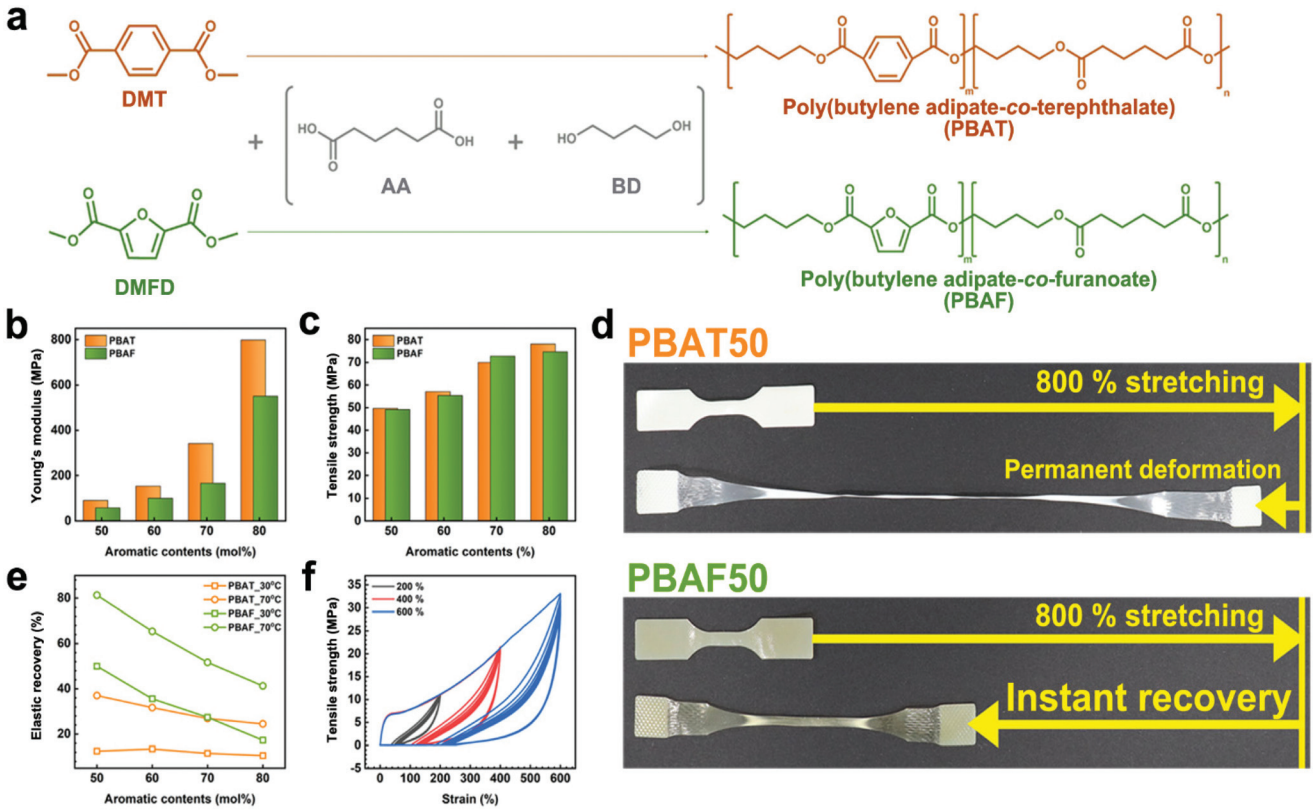

Fig. 1 (a) Synthesis of terephthalate-based poly(butylene adipate-*co*-terephthalate) (PBAT) and furanoate-based poly(butylene adipate-*co*-furanoate) (PBAF). Comparative analysis of (b) Young's modulus and (c) tensile strength. (d) Visual comparison of the elastic recovery of PBAT50 and PBAF50. (d) Elastic recovery test of PBATs and PBATs (at 30 °C (square) and 70 °C (circle)) with different aromatic contents. (f) Hysteresis test on PBAF50 at 200%, 400%, and 600% strains.

of PBAF to uniaxial stretching at high strains, *i.e.*, tensile strength. It is evident from Fig. 1e that the elastic recovery of PBATs at 30 °C over 12 h is as low as 10% and does not exceed 40% when the heating temperature was increased to 70 °C for the same duration. However, particularly for PBAF50, recoveries of 50% at 30 °C and 81% at 70 °C were observed; these are 4.0 and 2.2 times, respectively, greater than those of PBAT50. In the hysteresis tests, the highly elastic PBAF50 exhibited a slight drop in the ultimate tensile strength from 11.0 to 10.8 MPa (−1.1%), 21.2 to 20.3 MPa (−4.2%), and 33.1 to 28.6 MPa (−13.6%) after 10 cycles of 200%, 400%, and 600% strains, respectively (Fig. 1f). Such remarkable elasticity of PBAF50 seems to be derived from an entropy spring of the semi-rigid chain structure. As is known, stretched and oriented polymeric chains decrease the entropy which stimulates chains to recover their recoiled state upon unloading. Then, the symmetric and planar TPA moiety stabilizes the lateral packing of the aligned chains, disturbing the elastic recovery. On the other hand, the asymmetric FDCA moiety prefers recoiling to packing, resulting in reversible deformation. In addition, the immediate ring-flip of the furan ring accelerates the entropy recovery. Thus, from the long-term perspective, PBAFs have superior durability compared to PBATs.

The elasticity of polymers is determined not only from their chemical structure but also by the extent of entanglement with the neighboring chains. The entangled state can be traced using a rheological approach. Fig. 2 presents the rheological properties of molten PBAT50 and PBAF50 at 220 °C. It should be noted that PBAF50 has higher complex viscosity (η^*) and storage modulus (G') compared to PBAT50 over the entire frequency range observed (Fig. 2a). Generally, the rheological properties are predominantly affected by three factors: chemical structure of the chain (chain rigidity), size of the chain (molecular weight), and degree of entanglement (physical network). If the molecular weight difference of the comparative groups is negligible, the rheological parameters are commonly proportional to the chain rigidity. However, an opposite trend was observed in our case, indicating that PBAF50 possesses a stronger physical network compared to PBAT50 in the molten phase. Generally, the physical network is created by either a heterogeneous structure or a spatial entanglement of the chains.[52] The former can be ascertained by the evaluation of yield stress (τ_y), which represents the minimum energy required to collapse the heterogeneous structure.[53] It is clear from the Casson plots (Fig. 2b) that τ_y values of both the polymers are close to zero, signifying only a little heterogeneity in the molten state. Accordingly, the higher G' of PBAF50 as com-

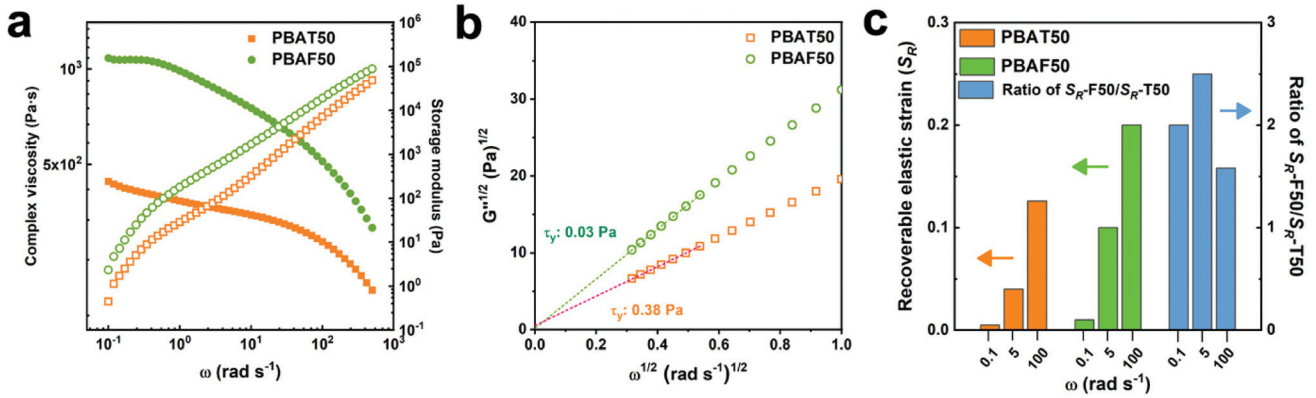

Fig. 2 Rheological properties of PBAT50 and PBAF50 at 220 °C: (a) complex viscosity (η^*) and storage modulus (G') in the angular frequency range 0.05–500 rad s^{-1}. (b) Casson plot for obtaining the yield stress (τ_y), and (c) recoverable elastic strains (S_R) of PBAT50 and PBAF50 and their ratios (S_R-F50/S_R-T50).

pared to PBAT50 can be exclusively ascribed to a higher number of chain entanglement. It is conjectured that the asymmetric and distorted FDCA can inter-diffuse and entangle with the aliphatic segments more efficiently as compared to the rigid TPA. In addition, the relatively polar nature of oxygen-containing FDCA contributes further to the enhanced intermolecular interaction and strengthened chain entanglement.[41] As a result, the recoverable elastic strain (S_R), a quantitative indicator of the rheological elasticity, in PBAF50 is twice that in PBAT50 at various frequencies (Fig. 2c).[54]

Structural and spectroscopic analysis of chemical and enzymatic degradation

The prominent effects of different aromatic structures can be better understood from the degradation in two different media and the weight loss as a result of the degradation (Fig. 3a and b). NaOH (1 M) at pH 13.4 was used as the chemical medium to accelerate the degradation. PBAF50 and PBAF70 were degraded by 60% and 49%, respectively, of their original weight within 6 days. These were 2 and 7 times, respectively, higher than the corresponding PBAT compositions (Fig. 3a). A similar trend in thickness reduction was also observed (Fig. S5†).

The faster degradation of PBAFs than PBATs originates from the inherent structural irregularity in the distorted and asymmetric FDCA. In contrast, the planar TPA with the benzene ring has a compact stacking of polymer chains, which severely impedes the degradation. Accordingly, two distinct tendencies can be observed in the chemical degradation: (1) high degradation rate of PBAFs compared to PBATs and (2) increased degradation rate at the lower ring fraction. Probably, these trends are strongly related to the penetration rate of hydroxyl anions (Fig. 3a).

During the enzymatic degradation using *Thermomyces lanuginosus* lipase (TLL), interestingly, PBAF50 underwent degradation without any trend, similar to the chemical degradation (Fig. 3b). In contrast to hydroxyl anions, TLL lipase is a highly selective catalyst owing to its size. TLL is a single chain protein consisting of 269 amino acids and has a molecular weight of 31 700 g mol^{-1}. It is spherical in shape, with an effective radius of ~50 Å.[55] Compared to hydroxyl anions (effective ionic radius of 0.1 Å),[56] TLL is an eminently bulky complex with a strong tendency to form bimolecular aggregates. Therefore, the enzymatic hydrolysis is not simply triggered by a physical penetration of the enzymes but is triggered by the enzyme specificity that originates upon the precise docking of the substrate onto oriented active sites on the enzyme; the precise docking accelerates specific reactions. In this regard, PBAF50 is the only polymer that satisfies the criterion of enzyme specificity. The peculiar morphology of the degraded PBAF50 reveals that the TLL enzymes attacked only those regions of the polymer chain in which the structural density or chain conformation was favorable for coordination with the enzyme molecules (Fig. 3b).

The enzyme specificity of PBAF50 can be confirmed from its structural analysis (Fig. 4). In the first heating scan in differential scanning calorimetry (DSC) (Fig. 4a and b), both the copolyesters exhibit two melting endotherms (T_{m1} and T_{m2}), which are representative of the crystalline structures of the aliphatic- and aromatic-rich phases, respectively. With an increase in the aromatic ring content, the peak position of T_{m1} remains almost constant at about 55 °C whereas that of T_{m2} increases drastically (*i.e.*, strongly dependent on the aromatic content) for both the copolyesters, indicating a substantial contribution of the aromatic ring to the crystalline phase (Fig. 4a and b). T_{m2} of PBAFs is about 50 °C lower than that of PBATs for the same aromatic contents, and, moreover, the dominance of the aromatic content is comparatively low. The heats of fusion at T_{m1} and T_{m2} (ΔH_{m1} and ΔH_{m2}) for the two copolyesters were compared (Fig. 4c and Table S4†). While ΔH_{m2} exceeds ΔH_{m1} at all the compositions in PBATs, the trend of ΔH_{m1} and ΔH_{m2} at 50 and 60 mol% of the aromatic content in PBAFs is different (Fig. 4d). In particular, for PBAF50, the crystalline phase is predominantly composed of the aliphatic component, with higher ΔH_{m1}. This structural difference between the two copolyesters can be determined from the different crystallizabilities of TPA and FDCA. As

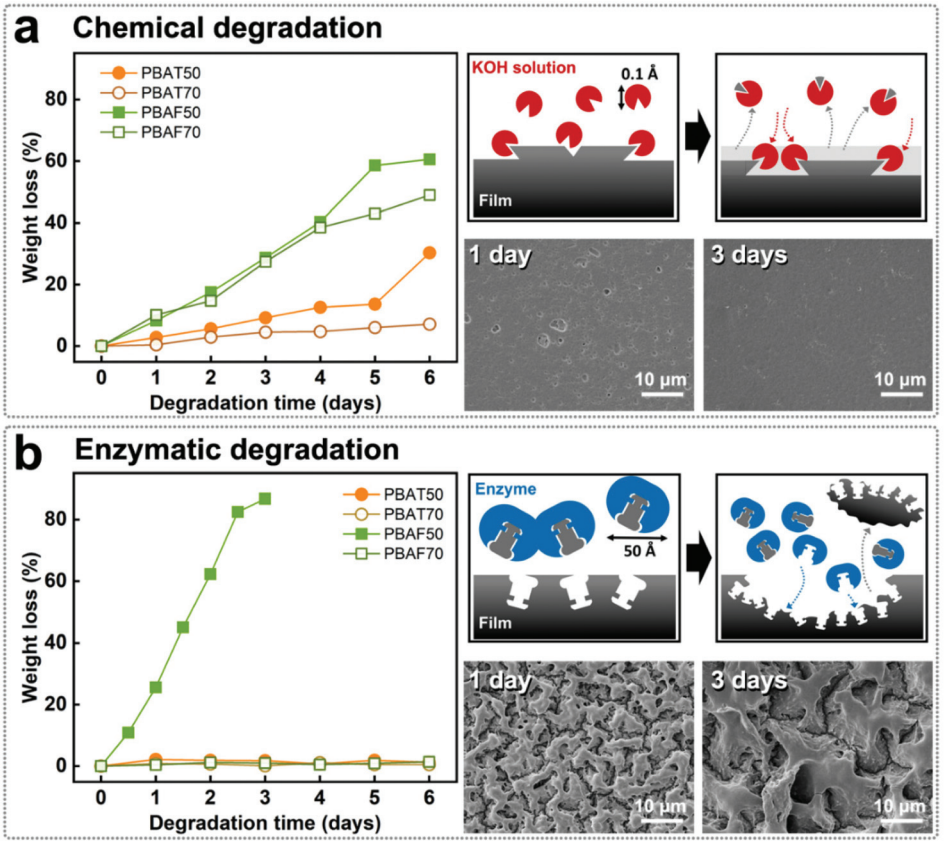

Fig. 3 (a) Chemical and (b) enzymatic degradation of PBATs and PBAFs at ring fractions of 50 and 70 mol% showing weight reduction, schematic of degradation, and SEM images of degraded samples.

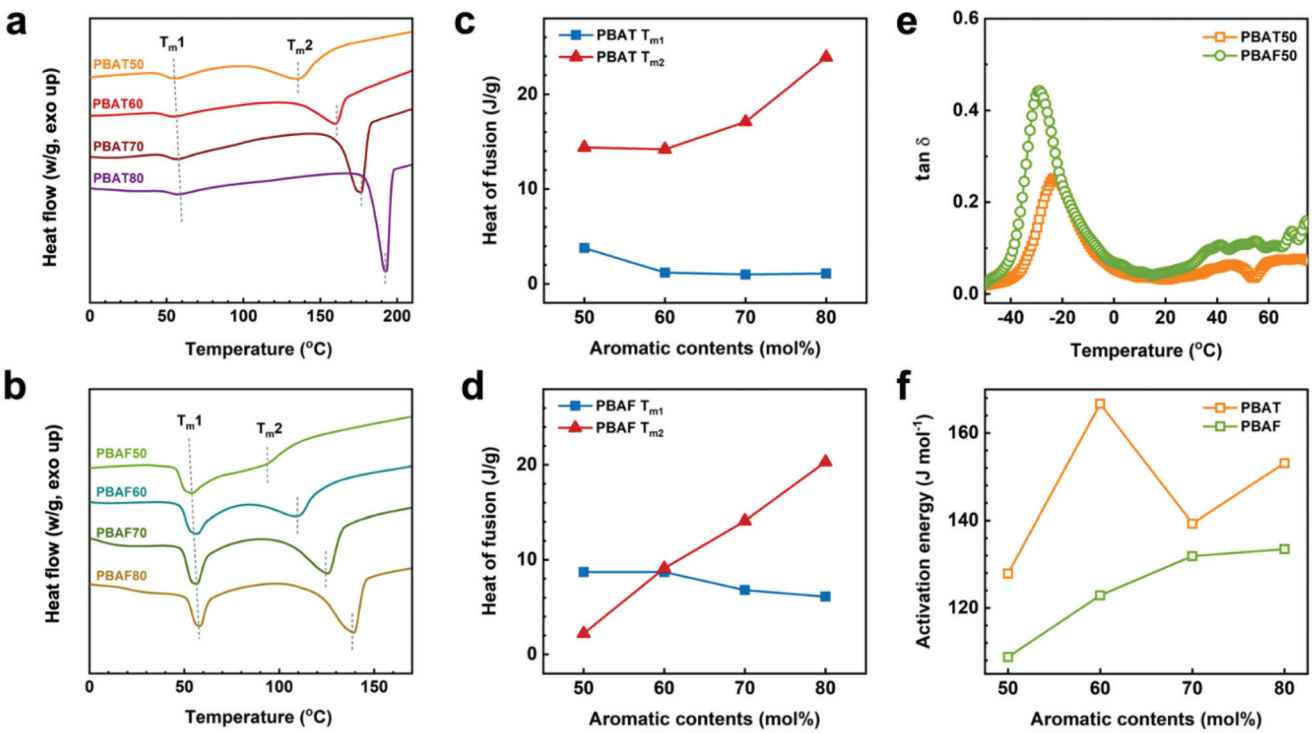

Fig. 4 1st heating scan of (a) PBATs and (b) PBAFs. Heats of fusion of (c) PBATs and (d) PBAFs. (e) Loss factor (tan δ) curves of PBAT50 and PBAF50 at a frequency of 1 Hz. (f) Activation energies (E_a) of PBATs and PBAFs at various aromatic contents calculated using the Arrhenius equation.

expected, the former promotes rapid crystallization due to the favorable π–π stacking of the benzene rings, while the latter undergoes a relatively slow crystallization due to the poor packing of distorted furan rings. Thus, low FDCA contents enable aliphatic chains to crystallize completely over a long time, depending on their molecular potential. It is because of this that an overwhelming ΔH_{m1} of PBAF50 is obtained. Moreover, the structure of PBAF50 with an evidently larger aliphatic crystalline phase supports the enzymatic selectivity.

Apart from the crystalline phase-dependent microstructure, a conformational change of the individual chains through a segmental motion significantly influences the enzyme selectivity during the degradation. An easier conformational change of the polymer chains provides better coordination with the enzyme, thereby leading to the enzymatic selectivity. The segmental motion of the chain and the relative conformational change can be explained based on the DMA (Fig. 4e and f). The peak position of loss tangent ($\tan\delta$) indicates the glass transition temperature (T_g) of each polymer.[57] Thus, the peak intensity (*i.e.*, the $\tan\delta$ value) of PBAF50 (0.44) is almost twice that of PBAT50 (0.25). Theoretically, a higher $\tan\delta$ value corresponds to a higher T_g value and less solid-like characteristics of a polymer owing to the enhanced segmental motion of the chains.[58] In this regard, it can be expected that the presence of asymmetric FDCA aids in active conformational changes during the hydrolysis. The fact that the favorable chain motion of PBAFs imparts enzyme specificity can be quantitatively confirmed from the activation energy (E_a) of the segmental motion. Fig. 4f and Fig. S6† show the Arrhenius plots for calculating the activation energies. The lower E_a values of PBAFs compared to PBATs over the entire 50–80 mol% ring fraction confirm that the activation of the segmental motion of the asymmetric FDCA-containing chains is more facile. Apart from the kinetic motion of the polymer chains, the furan ring also enhances the chemical affinity between the polar active sites of the enzymes and PBAF chains due to the existence of a polar oxygen atom. To evaluate the polar interactions, we calculated the theoretical solubility parameters of PBAF50 and PBAT50 using the Van Krevelen group contribution method (Fig. S7 and Table S5†).[59] Such theoretical parameters offer an indirect evidence of the chemical affinity between the polymers and the enzymes possessing numerous polar functional groups. It is worth noting that the polar (δ_p) and hydrogen bonding (δ_h) terms of the individual solubility parameters and the resulting total solubility parameter noticeably increase upon replacing TPA with FDCA. Particularly, δ_h at a ring fraction of 50 mol% for PBAF50 (δ_h = 8.9) is 1.3 times that for PBAT50 (δ_h = 6.7). This is because of the enhanced polarity originating from the oxygen-containing furan ring. From the viewpoints of the kinetic motion and thermodynamic affinity of PBAF50, it is believed that the enzyme preferably draws the ester groups adjacent to the polar furan ring. Additionally, the segmental motion of PBAF, which has a low E_a, favors the conformational change and imparts the enzymatic specificity.

Using advanced Fourier transform infrared (FT-IR) spectroscopy, another crucial clue to the enzymatic selectivity of PBAF50 during its *ex-situ* enzymatic degradation was obtained —hydrolysis of the ester groups adjacent to the furan ring triggered the enzymatic degradation. Fig. 5a shows the FT-IR spectrum on each day of the enzymatic degradation of PBAF50; the FT-IR spectra during the chemical degradation of PBAF50 and PBAT50 are also shown in Fig. S8† for comparison. The FT-IR spectra of the chemically and enzymatically hydrolyzed specimens were collected at intervals of 24 and 12 h, respectively. No significant changes in the spectrum were observed during the chemical degradation, probably because the hydrolyzed chains rapidly diffuse into the KOH solution and rarely remain on the specimen surface; this was further confirmed from the morphology observed by scanning electron microscopy (SEM, Fig. 3a). In contrast to chemical degradation, significant changes in the spectrum were observed during the enzymatic degradation. The intensity of the carbonyl peak (C═O) of PBAF50 at 1720 cm^{-1} drastically decreased with increasing time of degradation, along with the simultaneous appearance of a new carbonyl peak at around 1662 cm^{-1} from the hydrolyzed PBAF (Fig. 5a); the intensity of the new peak also increased with degradation time. Also, the peak increase in C═C at 1574 cm^{-1} and the peak increase/shift in ═C–O–C═ at 1223 and 1024 cm^{-1} of the furan ring indicate that the ester groups of FDCA are prone to hydrolysis during the enzymatic degradation. To the best of our knowledge, in the field of biodegradable polymers, this is the first evidence of the participation of FDCA in enzymatic degradation.

To further investigate the degradation mechanism of PBAF50, the time-dependent sequential changes in the FT-IR peaks were clarified using advanced analytical tools such as 2DCOS. 2DCOS is one of the most powerful and versatile spectral analysis tools that can establish the sequence of spectral changes under a given condition (in our case, the degradation time is a perturbation factor for the spectral change).[60] Synchronous and asynchronous 2DCOS obtained from the transient IR spectra of PBAF50 could identify the coincidental and sequential changes in the spectral intensities (Fig. 5b). With the exception of diagonally positive *autopeaks* (a result of the autocorrelation function of intensity variation) in synchronous 2DCOS, the positive cross peaks (red) imply that the intensities of two bands follow the same trend (either increasing or decreasing), whereas the negative cross peaks (blue) imply that the intensities of two bands follow the opposite trend (one is increasing while the other is decreasing). When designated cross-peaks from the synchronous spectrum match the sign of the asynchronous spectrum, the intensity change on the *x*-axis occurs before that on the *y*-axis and *vice versa*.

Fig. 5b shows the representative 2DCOS of PBAF50 during the enzymatic degradation; the remaining spectra are presented in Fig. S9.† The peak assignments for each matrix are summarized in Table S6.† The overall sequence of the peak transition (Fig. 5c) during the enzymatic degradation of PBAF50 is as follows: 1717↓ > 1731↓ > 1654↑ > 1583↓ > 1507↑ > 1163↓ > 1036↑ > 1127↓ > 1232↑ > 1283↑ > 1574↑ > 1149 cm^{-1}↑. As evident from the initial stages of degradation, carbonyls are separated into 1717, 1731, and 1654 cm^{-1}, which correspond to C═O adjacent

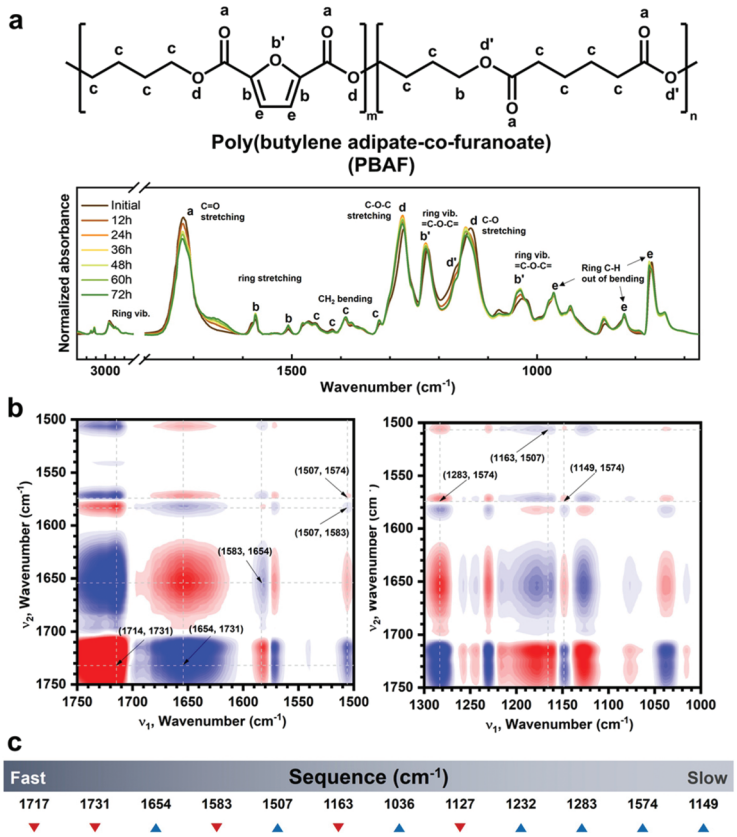

Fig. 5 (a) One-dimensional FT-IR spectra of PBAF50 during enzymatic degradation. Two-dimensional correlation spectroscopy (2DCOS) analysis to confirm the degradation sites and to obtain sequential information on degradation. (b) Homogeneous (left) and heterogeneous (right) synchronous 2DCOS spectra. (c) Sequence of peak transition during degradation.

to the furan ring, C=O from the aliphatic segment, and carbonyl from carboxylic acid, respectively. The carboxylic acid is formed because of the ester hydrolysis of FDCA. The interesting aspect of this spectral sequence is that the change in carbonyl bonds near the furan ring triggered the entire degradation of PBAF50. In other words, the participation of the ester groups on the ring triggers the entire hydrolysis, giving rise to enzymatic specificity. Conventionally, the enzymatic degradation of some copolyesters has been exclusively explained by the hydrolysis of the aliphatic region, while ignoring the role of the aromatic phase. However, this study confirms that if the aromatic ring segment can actively participate in degradation owing to a lower E_a value for the conformational change, as in PBAF50, the hydrolysis of ester groups neighboring the ring structure is the first step in the enzymatic degradation.

Conclusions

In summary, it is shown that PBAF has significant merits in terms of elastic performance as well as biodegradability, compared to its terephthalic counterpart, PBAT. Upon uniaxial stretching, PBAT lost its mechanical properties due to permanent deformation, while PBAF exhibited remarkable recovery upon release, ensuring its long-term durability. The advantages of PBAF was further highlighted in its enzymatic degradation with a ring fraction of 50 mol%. In the TLL-induced degradation, PBAF solely underwent hydrolysis, highlighting the enzymatic specificity. Such remarkable elasticity and enzymatic degradability of PBAF can be attributed to the structural characteristics of the furan ring. The rheological analyses confirmed that the asymmetric and semi-rigid FDCA-based PBAF underwent a larger number of chain entanglement than the rigid TPA-based PBAT, ultimately developing stronger elasticity. During the degradation, the ease of the conformational change of the PBAF chains, owing to its low E_a, enabled the hydrolysis of the ester groups neighboring the furan ring, thereby triggering the successive enzymatic degradation. At the current state, PBAF production is incomparable to PBAT since FDCA is in economic disadvantage to TPA in terms of cost, production and technology. The importance of successful petroleum counterparts, however, emphasizes the potential of FDCA to continue its research and become a potential core component in biodegradable plastics.

Experimental

Materials

Dimethyl-2,5-furandicarboxylate (DMFD, 99.7%) was purchased from Apollo Scientific (UK). Adipic acid (AA, 99%),

dimethyl terephthalate (DMT, 99%), 1,4-butanediol (BD, 99.5%), titanium(IV) butoxide (TBT, 97%), deuterated chloroform ($CDCl_3$, 99.5 atom%), trifluoroacetic acid-d (TFA, 99.5 atom%), high purity chloroform (HPLC grade, $CHCl_3$), and *Thermomyces lanuginosus* lipase were purchased from Sigma-Aldrich (USA). Sodium phosphate monobasic and dibasic (98.0%–102.0%) were purchased from GENERAY Biotech (China). All the chemicals were used as received without further purification.

Synthesis of PBAT and PBAF copolyesters

PBAF and PBAT copolyesters were synthesized by a conventional two-step melt polymerization method. For the synthesis of PBAF50, DMFD (0.183 mol, 33.64 g), AA (0.183 mol, 26.70 g), and BD (0.585 mol, 52.69 g) were injected into a 1 L reactor placed on a heating mantle equipped with a condenser, N_2 line, and mechanical stirrer. The reactor was purged with N_2 gas to remove H_2O and O_2, in order to prevent oxidation and depolymerization. The esterification was initiated by heating the mixture to 140 °C, along with mechanical stirring at 150 rpm. When the monomers were fully molten, TBT (0.05 mol% relative to the total molarity of diacids) was added. The temperature was gradually increased to 180 °C at 2 °C min^{-1} and held for 2 h. Following this, the temperature was increased to 210 °C and held at this temperature for another 2 h. The esterification product was directly transferred to a customized glass reactor equipped with a mechanical stirrer and a vacuum line. The reactor was placed in an oil bath to initiate the polycondensation. Starting at 160 °C with a mechanical stirring of 50 rpm, the temperature was gradually increased to 240 °C at a rate of 2 °C min^{-1} while the pressure was gradually decreased. The reaction was held for 2 h while maintaining the vacuum at 100 mTorr. The resulting product was quenched in cold water and dried in a vacuum oven at 60 °C for 24 h. All the samples were analyzed without any further purification, and no antioxidants and anti-discolorants were used.

Characterization

The number-average molecular weight (M_n), weight average molecular weight (M_w), and polydispersity index (PDI = M_n/M_w) were determined using size exclusion chromatography (SEC, ACQUITY APC XT, Waters Corp., USA); the instrument was equipped with a ACQUITY refractive index detector. Chloroform was used as an eluent at a flow rate was 0.6 mL min^{-1}, and the column temperature was fixed at 40 °C. M_n, M_w, and PDI were calculated after calibrating with polystyrene (PS) standards. ^{1}H NMR spectra were obtained on an AVANCE NEO 500 (Bruker, USA) spectrometer at 500 MHz. $CDCl_3$ and tetramethylsilane (TMS) were used as the solvent and internal standard, respectively. Due to the poor solubility of PBAT80 in $CDCl_3$, TFA was used as the solvent. Sixteen scans with 65 536 data points were acquired for each ^{1}H NMR spectrum.

The mechanical properties of the synthesized polyesters were measured by a universal testing machine (UTM, Instron 5943, USA). The synthesized copolyesters were hot-pressed at 150–210 °C at 100 bar for 5 min and quenched in cold water. After drying, films (0.5 mm thickness) were cut in the shape of a dumbbell using a cutting die (ASTM D412). All the specimens were conditioned at 25 °C and 20% relative humidity for 48 h; measurements were carried out under the same conditions. The crosshead speed was 100 mm min^{-1}, and each specimen was tested more than 10 times. In order to evaluate the elastic recovery behavior, each dumbbell-shaped specimen was stretched up to 400% using a customized stretching machine and then conditioned at 30 °C for 24 h while maintaining the stretched state. After annealing, the stretched sample was released in an ice water bath for quenching, to minimize the instantaneous recovery. Finally, the extents of elastic recovery of the quenched samples were measured after stress relaxation at 30 or 70 °C for 3 h. For comparing the instant elastic recovery and hysteresis of PBAF50 and PBAT50, the dumbbell-shaped specimens were stretched up to 800% using UTM at a crosshead speed of 100 mm min^{-1} and then released immediately. Particularly for the highly elastic PBAF50, the cyclic hysteresis test was conducted with 10 cycles of 200%, 400%, and 600% strains. The crosshead speed of each hysteresis test was fixed at 100 mm min^{-1}.

Thermal behaviors of the synthesized copolyesters were investigated by differential scanning calorimetry (TA instrument, Q200, USA) under a N_2 atmosphere. The temperature was varied from −50 to 250 °C at a scan rate of 10 °C min^{-1}. The measurements were carried out with 5 mg of each sample. The dynamic mechanical properties of the samples were analyzed using a PerkinElmer DMA 8000 (USA) in the temperature range of −50–150 °C at a heating rate of 3 °C min^{-1}. All the measurements were carried out in tension mode at fixed frequencies of 0.1, 1, 5, and 20 Hz, and at 0.02% strain. The specimens were prepared in the shape of a rectangular bar of dimensions 5 × 0.5 × 10 mm by a hot-pressed method, mentioned in the UTM analysis. The chemical structures of the synthesized and degraded copolyesters were analyzed by FTIR (iS50-FTIR, USA). For each spectrum, 258 scans were collected with a spectral resolution of 4 cm^{-1}. The background of air was subtracted before each measurement. Before analysis, each spectra were smoothed to 5 points and baseline correction was done with 11 points. Then the data were normalized in accordance with PBAT50 and PBAF50 for each series, respectively. For the attenuated total reflection (ATR) measurements, the film or dumbbell-type specimen was placed on the surface of a diamond crystal plate. 2DCOS analysis was conducted using 2DShige program (freely downloadable software developed by Prof. Shigeaki Morita, Osaka Electro-Communication University, Japan). Field-emission SEM was performed on a Tescan MIRA3 (Czech Republic) microscope to view the degradation morphologies of the synthesized copolyesters. Before the analysis, the samples were coated with platinum for fine observation. The rheological properties of PBAT50 and PBAF50 were measured by the dynamic frequency sweep test using a rotational rheometer MCR 302 (Anton Paar, Austria) with a 25 mm parallel plate. The gap distance between the plates and the strain were 1 mm and 10%, respectively. The oscillation frequency sweep was carried out at 220 °C in

the angular frequency range of 0.05–500 rad s^{-1}. The disc type specimens were prepared by the hot-press method as mentioned above.

Chemical and enzymatic degradation analysis

All the samples were prepared as 0.2 mm thick films using the hot-press method mentioned in UTM analysis. The specimens were cut in the shape of a dumb-bell using a cutting die (ISO 37) to maintain the same surface area. The weight was fixed at 0.25 ± 0.05 g. Chemical degradation was conducted in aqueous 1 M NaOH solution at pH 13.4. Enzymatic degradation was performed in 0.1 M phosphate buffer of pH 6.5 using lipase from *Thermomyces lanuginosus*.

For each medium, the specimen was placed in a vial (5 ml) and shaken at 50 °C at 80 rpm for 6 days. For the enzymatic degradation, the medium was replenished every day to ensure the maximum enzyme activity. The degradation rate was determined by weight and thickness losses, and the structural transition during the degradation was observed through FT-IR spectroscopy.

Conflicts of interest

There are no conflicts to declare.

Acknowledgements

This research was supported by the Korea Research Institute of Chemical Technology (KRICT) Core Project (SS2042-10), Bio-Industrial Technology Development Program (20008628) funded by the Ministry of Trade, Industry & Energy (MI, Korea), the National Research Foundation of Korea (NRF-2020R1C1C1009340, 2020R1C1C1003665) and the Korea Institute of Energy Technology Evaluation and Planning (KETEP) and the Ministry of Trade, Industry & Energy (MOTIE) of the Republic of Korea (No. 20194010201840).

Notes and references

1 R. Siddique, J. Khatib and I. Kaur, *Waste Manage.*, 2008, **28**, 1835.
2 S. Wong, N. Ngadi, T. Abdullah and I. Inuwa, *Renewable Sustainable Energy Rev.*, 2015, **50**, 1167.
3 Y. Zheng, E. K. Yanful and A. S. Bassi, *Crit. Rev. Biotechnol.*, 2005, **25**, 243.
4 M. Eriksen, L. C. Lebreton, H. S. Carson, M. Thiel, C. J. Moore, J. C. Borerro, F. Galgani, P. G. Ryan and J. Reisser, *PLoS One*, 2014, **9**, e111913.
5 Y. Chae and Y.-J. An, *Environ. Pollut.*, 2018, **240**, 387.
6 S. Curia, A. Biundo, I. Fischer, V. Braunschmid, G. M. Gübitz and J. F. Stanzione III, *ChemSusChem*, 2018, **11**, 2529.
7 S. Lambert and M. Wagner, *Chem. Soc. Rev.*, 2017, **46**, 6855.
8 T. P. Haider, C. Völker, J. Kramm, K. Landfester and F. R. Wurm, *Angew. Chem., Int. Ed.*, 2019, **58**, 50.
9 Y. Tokiwa and T. Suzuki, *Nature*, 1977, **270**, 76.
10 M. Rabnawaz, I. Wyman, R. Auras and S. Cheng, *Green Chem.*, 2017, **19**, 4737.
11 T. Kim, J. M. Koo, M. H. Ryu, H. Jeon, S.-M. Kim, S.-A. Park, D. X. Oh, J. Park and S. Y. Hwang, *Polymer*, 2017, **132**, 122.
12 S.-A. Park, H. Jeon, H. Kim, S.-H. Shin, S. Choy, D. S. Hwang, J. M. Koo, J. Jegal, S. Y. Hwang, J. Park and D. X. Oh, *Nat. Commun.*, 2019, **10**, 1.
13 J. M. Koo, J. Kang, S.-H. Shin, J. Jegal, H. G. Cha, S. Choy, M. Hakkarainen, J. Park, D. X. Oh and S. Y. Hwang, *Compos. Sci. Technol.*, 2020, **185**, 107885.
14 S. Rameshkumar, P. Shaiju, K. E. O'Connor and R. Babu, *Curr. Opin. Green Sustainable. Chem.*, 2020, **21**, 75.
15 R. Herrera, L. Franco, A. Rodríguez-Galán and J. Puiggalí, *J. Polym. Sci., Part A: Polym. Chem.*, 2002, **40**, 4141.
16 L. Zhao and Z. Gan, *Polym. Degrad. Stab.*, 2006, **91**, 2429.
17 F. V. Ferreira, L. S. Cividanes, R. F. Gouveia and L. M. Lona, *Polym. Eng. Sci.*, 2019, **59**, E7.
18 J. Jian, Z. Xiangbin and H. Xianbo, *Adv. Ind. Eng. Polym. Res.*, 2020, **3**, 19.
19 H. Moustafa, C. Guizani, C. Dupont, V. Martin, M. Jeguirim and A. Dufresne, *ACS Sustainable Chem. Eng.*, 2017, **5**, 1906.
20 A. M. Díez-Pascual and A. L. Díez-Vicente, *RSC Adv.*, 2015, **5**, 93095.
21 O. Weizman, A. Dotan, Y. Nir and A. Ophir, *Polym. Adv. Technol.*, 2017, **28**, 261.
22 T. Kijchavengkul, R. Auras, M. Rubino, M. Ngouajio and R. T. Fernandez, *Chemosphere*, 2008, **71**, 942.
23 F. Touchaleaume, L. Martin-Closas, H. Angellier-Coussy, A. Chevillard, G. Cesar, N. Gontard and E. Gastaldi, *Chemosphere*, 2016, **144**, 433.
24 A. P. Bilck, M. V. Grossmann and F. Yamashita, *Polym. Test.*, 2010, **29**, 471.
25 K. Fukushima, M.-H. Wu, S. Bocchini, A. Rasyida and M.-C. Yang, *Mater. Sci. Eng., C*, 2012, **32**, 1331.
26 G. F. Santana-Melo, B. V. Rodrigues, E. da Silva, R. Ricci, F. R. Marciano, T. J. Webster, L. M. Vasconcellos and A. O. Lobo, *Colloids Surf., B*, 2017, **155**, 544.
27 A. Arslan, S. Çakmak, A. Cengiz and M. Gümüşderelioğlu, *J. Biomater. Sci., Polym. Ed.*, 2016, **27**, 1841.
28 D. Savostianoff and S. Didier, *Inf. Chim.*, 1993, **352**, 119.
29 R. Wolkowski-Tyl, T. Chin and H. D. A. Heck, *Drug Metab. Dispos.*, 1982, **10**, 486.
30 P. Engel, K. K. Brandt, L. H. Rasmussen, R. G. Ovesen and J. Sørensen, *Chemosphere*, 2007, **67**, 202.
31 S. Qi, X. Wang, X. Xu and Q. Xiang, *J. Hyg. Res.*, 2002, **31**, 10.
32 N. Scholz, *Chemosphere*, 2003, **53**, 921.
33 B.-J. Chen, Y.-X. Yuan and H.-P. Wang, *J. Fish. Sci. China*, 2001, **8**, 73.
34 A. Eerhart, A. Faaij and M. K. Patel, *Energy Environ. Sci.*, 2012, **5**, 6407.

35 G. Z. Papageorgiou, D. G. Papageorgiou, Z. Terzopoulou and D. N. Bikiaris, *Eur. Polym. J.*, 2016, **83**, 202.
36 A. Sousa, N. Guigo, M. Pożycka, M. Delgado, J. Soares, P. Mendonca, J. Coelho, N. Sbirrazzuoli and A. Silvestre, *Polym. Chem.*, 2018, **9**, 722.
37 A. F. Sousa, C. Vilela, A. C. Fonseca, M. Matos, C. S. Freire, G.-J. M. Gruter, J. F. Coelho and A. J. Silvestre, *Polym. Chem.*, 2015, **6**, 5961.
38 F. H. Isikgor and C. R. Becer, *Polym. Chem.*, 2015, **6**, 4497.
39 R. De Clercq, M. Dusselier and B. Sels, *Green Chem.*, 2017, **19**, 5012.
40 S. K. Burgess, J. E. Leisen, B. E. Kraftschik, C. R. Mubarak, R. M. Kriegel and W. J. Koros, *Macromolecules*, 2014, **47**, 1383.
41 F. A. Kucherov, E. G. Gordeev, A. S. Kashin and V. P. Ananikov, *Angew. Chem., Int. Ed.*, 2017, **56**, 15931.
42 S. Peng, L. Wu, B.-G. Li and P. Dubois, *Polym. Degrad. Stab.*, 2017, **146**, 223.
43 S. Weinberger, K. Haernvall, D. Scaini, G. Ghazaryan, M. T. Zumstein, M. Sander, A. Pellis and G. M. Guebitz, *Green Chem.*, 2017, **19**, 5381.
44 L. Papadopoulos, A. Magaziotis, M. Nerantzaki, Z. Terzopoulou, G. Z. Papageorgiou and D. N. Bikiaris, *Polym. Degrad. Stab.*, 2018, **156**, 32.
45 H. Hu, R. Zhang, J. Wang, W. B. Ying and J. Zhu, *Eur. Polym. J.*, 2018, **102**, 101.
46 K. Haernvall, S. Zitzenbacher, H. Amer, M. T. Zumstein, M. Sander, K. McNeill, M. Yamamoto, M. B. Schick, D. Ribitsch and G. M. Guebitz, *Biotechnol. J.*, 2017, **12**, 1600741.
47 I. Noda, *J. Mol. Struct.*, 2016, **1124**, 29.
48 Y. Park, S. Jin, I. Noda and Y. M. Jung, *J. Mol. Struct.*, 2018, **1168**, 1.
49 H. Moon, S. Choy, Y. Park, Y. M. Jung, J. M. Koo and D. S. Hwang, *Mar. Drugs*, 2019, **17**, 318.
50 R. Herrera, L. Franco and A. Rodríguez-Galán, *J. Polym. Sci., Part A: Polym. Chem.*, 2002, **40**, 4141.
51 J. C. Randell, *Polymer Sequence Determination*, Academic Press, New York, 1977.
52 Y. Eom and B. C. Kim, *Polymer*, 2014, **55**, 2570.
53 J. H. Yoon, S.-M. Kim, Y. Eom, J. M. Koo, H.-W. Cho, T. H. Lee, K. G. Lee, H. J. Park, Y. K. Kim, H.-J. Yoo, S. Y. Hwang, J. Park and B. G. Choi, *ACS Appl. Mater. Interfaces*, 2019, **11**, 46165.
54 F. Kim, B. Kwon, Y. Eom, J. E. Lee, S. Park, S. Jo, S. H. Park, B.-S. Kim, H. J. Im, M. H. Lee, T. S. Min, K. T. Kim, H. G. Chae, W. P. King and J. S. Son, *Nat. Energy*, 2018, **3**, 301.
55 R. Fernandez-Lafuente, *J. Mol. Catal. B: Enzym.*, 2010, **62**, 197.
56 Y. Marcus and R. Fernandez-Lafuente, *J. Chem. Phys.*, 2012, **137**, 154501.
57 J.-E. Lee, Y. Eom, Y.-E. Shin, S.-H. Hwang, H.-H. Ko and H. G. Chae, *ACS Appl. Mater. Interfaces*, 2019, **11**, 13665.
58 A. F. Lewis, *J. Polym. Sci., Part B: Polym. Lett.*, 1963, **1**, 649.
59 S.-A. Park, Y. Eom, H. Jeon, J. M. Koo, E. S. Lee, J. Jegal, S. Y. Hwang, D. X. Oh and J. Park, *Green Chem.*, 2019, **21**, 5212.
60 J.-E. Lee, Y. Eom, Y.-E. Shin, S.-H. Hwang, H.-H. Ko and H. G. Chae, *ACS Appl. Mater. Interfaces*, 2019, **11**, 13665.